analytical chemistry

Article

pubs.acs.org/ac

# Three-Color Fluorescence Cross-Correlation Spectroscopy for Analyzing Complex Nanoparticle Mixtures

Megan L. Blades,[†] Ekaterina Grekova,[†] Holly M. Wobma,[†,§] Kun Chen,[‡] Warren C. W. Chan,[‡] and David T. Cramb*,[†]

[†]Department of Chemistry, University of Calgary, 2500 University Drive NW, T3A 0J1, Calgary, Alberta, Canada

[‡]Institute of Biomaterials and Biomedical Engineering, Donnelly Centre for Cellular and Biomolecular Research, Chemistry, Materials Science and Engineering, and Chemical Engineering, University of Toronto, 160 College Street, Toronto, Ontario, Canada M5S 3E1

Supporting Information

**ABSTRACT:** Further insight toward the complex association and dissociation events of macromolecules requires the development of a spectroscopic technique that can track individual components, or building blocks of these macromolecules, and the complexes which they form, in real time. Three-color fluorescence cross-correlation spectroscopy (3C-FCCS) has been shown to track assemblies of three spectrally labeled species in solution. Here, we clearly show that 3C-FCCS is capable of distinguishing beads barcoded with quantum dots from free quantum dots in the background despite the 800-to-1 difference in concentration of these two components. The validation of this spectroscopic technique in combination with the development of barcode labels would enable one to start to investigate complex association and dissociation kinetics of macromolecules and nanomaterials during the assembly process.

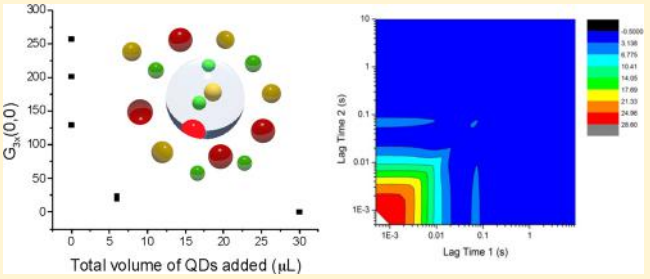


Understanding how biological and chemical molecules and structures interact with one another will have broad significance. Probing the interactions of proteins with other proteins or nucleic acid may lead to new diagnostics or therapeutics; and probing nanomaterials' interactions with one another may lead to faster and smaller electronic chips. While there has been much focus on developing the chemical principles for assembling two or more components together,[1] there are very limited techniques being developed that can monitor and track the assembly process.

One of the most promising technologies to monitor molecular assembly is spectroscopy, where each component is tagged with a different color fluorophore. As the components assemble together, one monitors the change in the fluorescence using single-molecule optical techniques. By monitoring the optical signal through time, we would be able to measure the real-time kinetics of the formation process. While this analytical strategy is simple conceptually, there are considerable challenges in extracting such a signal from a background of nonassociated building blocks, a main obstacle being cross talk free spectroscopic registration of the individual species. To date, only two techniques can provide unequivocal detection of spectrally tagged, multicomponent assemblies. These are multicolor Förster resonance energy transfer (MC-FRET)[2,3] and multicolor fluorescence cross-correlation spectroscopy[4−8] (MC-FCCS).

Since 2000, several elegant MC-FRET experiments have been reported.[2,3,8−10] They have used the one-donor, two-acceptor approach to interrogate multicomponent associations in a biological milieu. Spectral cross talk between channels and direct excitation of the acceptor molecules are problematic when using organic fluorophores as the labels. These issues are often surmountable with appropriate control experiments and/or the use of quantum dots (QDs) or lanthanide-based luminescent tags, the latter of which are spectrally sharp but tend to have low excitation cross sections. In an example of a lanthanide-based FRET approach, Kim et al. employed $Tb^{3+}$ as a donor for the first demonstration of a one-donor, three-acceptor FRET assay of ligands binding to the estrogen receptor.[9] Nevertheless, MC-FRET remains challenged by dynamic changes in the relative orientation of donor/acceptor combinations and direct excitation of acceptor fluorophores, both of which can obfuscate the reporting of binding events.

An alternative to MC-FRET is multicolor fluorescence cross-correlation spectroscopy.[4−6] In principle, MC-FCCS can report directly and rapidly on the assembly of multicomponent systems without the analysis complexity of MC-FRET. Complex reactions and assembly processes can be tracked in real time. In MC-FCCS, fluorescence intensity fluctuations result from fluorescently tagged molecules passing through an optically defined interrogation volume. These fluctuations are analyzed for temporal correlations and species with all labels register as a valid event. By monitoring the diffusion patterns of these species, MC-FCCS can also provide direct information on

**Received:** September 7, 2012
**Accepted:** October 11, 2012
**Published:** October 11, 2012



   dx.doi.org/10.1021/ac302572k | *Anal. Chem.* 2012, 84, 9623−9631

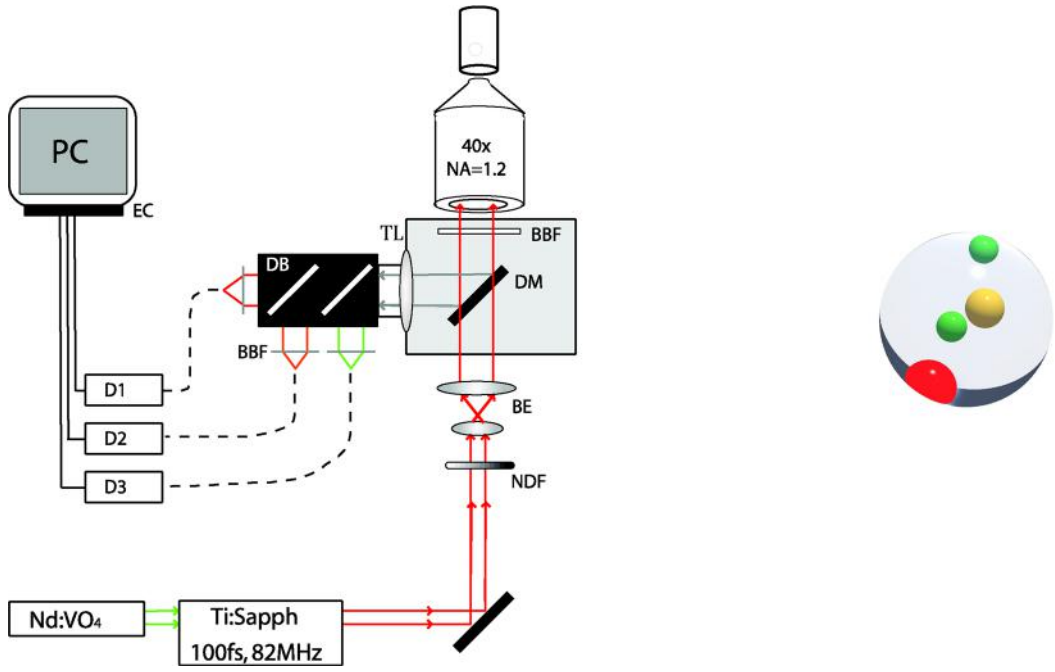


**Figure 1.** Experimental setup. Excitation beam (red) passes through a neutral density filter (ND), a beam expander (BE), a dichroic mirror (DM), and birefringent band filter (BBF) en route to a compound objective lens. Fluorescence is collected back through the objective lens, tube lens (TL), and directed to dichroic beam splitters for spectral selection. Light is collected into optical fibers and detected by avalanche photodiodes (D1–D3). The signals from the photodiodes are processed by an event counter (EC) and analyzed on a personal computer.

their concentration and size. Inspired by the pioneering coincidence analysis work of Heinze et al.[4] and of Hwang et al.,[5] we recently reported the first direct measurement of three-color (3C) FCCS signals with full temporal analysis.[6] To our knowledge, the three-color fluorescence cross-correlation spectroscopy (3C-FCCS) approach we developed is the only way to verify the existence of a three-color species directly.

In our previous work on 3C-FCCS, we demonstrated its application to multicolor nanobarcode particles (300 nm diameter polymer spheres loaded with quantum dots of three different colors)[11,12] and to track complex DNA assembly using three differently colored QDs.[6] We found that 3C-FCCS decays could be collected from 100 pM of nanobarcode particles and in less than 1 min for the DNA trimer assembly. There were very few free, single-color species in the background. In order to follow the kinetics of complex macromolecular or nanoparticle assembly/disassembly using MC-FCCS, one must have confidence that the concentration of assembled multicomponent species can be measured in situ where the free components are orders of magnitude greater in concentration. To test the capacity of MC-FCCS to accomplish this task, we chose to create a series of well-controlled experiments where three-color nanobarcode particles were mixed in solution with free and single emission color QDs. Since these solutions have defined ratios of free QDs to multicolor nanobarcode particles, the ability of MC-FCCS to accurately measure the concentrations of these components can be rigorously evaluated.

Here, we examined the capacity of 3C-FCCS to determine the concentration of three-color nanobarcode particles in solutions containing free QDs, which are 800× greater in concentration. We have validated both the experimental approach to 3C-FCCS measurements and the use of mathematical models for 3C-FCCS for analysis of complex nanoparticle solutions.

## MATERIALS AND METHODS

**Preparation of Nanobarcode Particles.** The three-color nanobarcode particles were prepared in a similar fashion to our previous work.[6,11,12] Their sizes were measured using dynamic light scattering (DLS) and scanning electron microscopy (SEM). Details can be found in the Supporting Information.

**Background Fluorescence Protocols.** CdSe core–ZnS shell streptavidin-coated QDs (Invitrogen) emitting at 525, 605, and 655 nm were used to add background fluorescence to solutions of three-color nanobarcode particles in the green, orange, and red detection channels, respectively. Details on these preparations and on control experiments can be found in the Supporting Information.

**Optical Setup.** Our optical setup is shown in Figure 1. All nanoparticles were excited by two-photon absorption. This has the advantages of simplifying the optics (no detection pinhole) and obviating the need to align multiple lasers for simultaneous excitation of different nanoparticles. Details of the optical configuration can be found in the Supporting Information.

**Theory.** As stated in our prior communication, the triple cross-correlation function has been previously defined by Heinze et al.:[4]

$$G_{3x}(\tau_1, \tau_2) = \frac{\langle \partial F_a(t) \partial F_b(t+\tau_1) \partial F_c(t+\tau_2) \rangle}{\langle F_a \rangle \langle F_b \rangle \langle F_c \rangle} \quad (1)$$

where the $F$'s are the fluorescence intensities in channels $a$, $b$, and $c$. The $\partial F$'s are the instantaneous difference from the time average $\langle F \rangle$'s; the $\tau$'s are the lag times between the channels. At short lag times the cross-correlation becomes constant, and its amplitude can be related to the average number of triply labeled species in the detection volume (see eqs 3–5).

When the fluctuation dynamics are dominated by diffusion through the interrogation volume, the triple cross-correlation matrix is expected to decay to zero with some characteristic


dx.doi.org/10.1021/ac302572k | Anal. Chem. 2012, 84, 9623–9631

time, $\tau_D$.[13] The functional form of that decay has recently been derived for one-color, two-photon excitation triple fluorescence correlations.[7] The equation for three-color FCCS should be analogous to that equation.

For the diagonal component, $(\tau_2 - \tau_1) = \tau_1 = \tau$ and eq 1 simplifies to

$$G_{3x}(\tau_1, \tau_2 - \tau_1) = G_{3x}(0, 0)\left(1 + \frac{8\tau^2}{3{\tau_D}^2} + 8\tau/3\tau_D\right)^{-1} \left(1 + \frac{\frac{8\tau^2}{3{\tau_D}^2}{r_0}^4}{{z_0}^4} + \frac{{r_0}^2}{{z_0}^2}\frac{8\tau}{3\tau_D}\right)^{-1/2} \quad (2)$$

where $\tau_D$ is the average residence time in the interrogation volume and $z_0$ and $\phi_0$ are the two-photon excitation (TPE) volume depth and waist, respectively. Details of the derivation of eq 2 are found in the Supporting Information.

In a diffusional regime, a plot of the cross-correlation matrix (eq 1) has previously shown that the variables $\tau_1$ and $\tau_2$ are independent and produce perpendicular contours.[6]

This is also true for the current study, as indicated by Figure 2. Thus, we are confident in using eq 2 to fit the 3C-FCCS the diagonal components of the decays to follow.

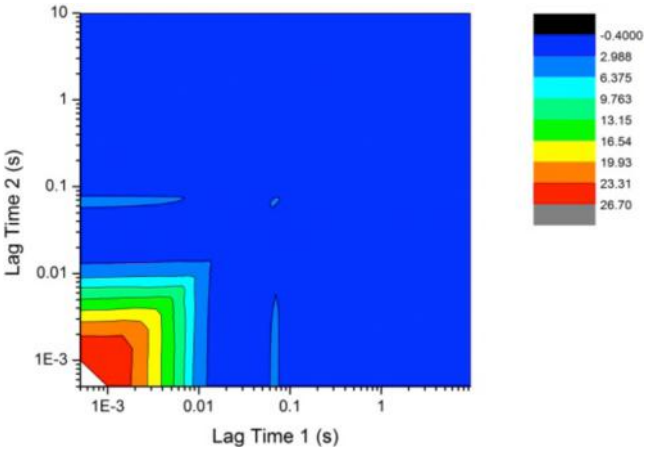


**Figure 2.** Contour plot of the full three-color cross-correlation decay for nanobarcode particles. The solution contained 200 pM particles and was excited at 50 mW as described in the text. The diagonal component of the plot represents data that follows eq 5. Note the square shape of the plateaus.

We and others have previously shown that the amplitude of the triple cross-correlation signal can be given by[4,6]

$$G_{3x}(0, 0) = \frac{\eta_a\eta_b\eta_c N_{abc}}{\sum_i \eta_{ai}N_{ai} \sum_j \eta_{bj}N_{bj} \sum_k \eta_{ck}N_{ck}} \quad (3)$$

where $N_{abc}$ is the average number of three-color species in the TPE volume. The sums in the denominator are over the particles, $i$, $j$, or $k$, that register in the spectrally defined color channels $a$, $b$, or $c$ (green, orange, and red), and $\eta$'s are the particle brightnesses (count rate/particle).

If there are only three-color nanobarcode particles, then $N_{abc} = N_{ai} = N_{bj} = N_{ck}$ and eq 3 simplifies to

$$G_{3x}(0, 0) = \frac{1}{{N_{abc}}^2} \quad (4)$$

This relationship has been verified and can be found in the Supporting Information. If a single-color free particle, $N_a$, is added to the solution and we consider particle brightness

$$G_{3x}(0, 0) = \frac{\eta_a\eta_b\eta_c N_{abc}}{(\eta_a' N_a + \eta_a N_{abc})(\eta_b N_{abc})(\eta_c N_{abc})} = \frac{\eta_a}{(\eta_a' N_a + \eta_a N_{abc})N_{abc}} = \frac{1}{\left(\frac{\eta_a'}{\eta_a}N_a + \frac{1}{\sqrt{G_{3x}(0,0)'}}\right)\left(\frac{1}{\sqrt{G_{3x}(0,0)'}}\right)} \quad (5)$$

where $G_{3x}(0, 0)'$ is the $G_{3x}(0, 0)$ value of three-color nanobarcode particles with no free QDs present (value derived from eq 4) and $\eta$ and $\eta'$ are the brightness of the free quantum dot and the three-color nanobarcode particle, respectively, in the equivalent detection channel. Brightnesses were calculated using autocorrelation amplitudes and the average count rates for all the particles at 50 mW laser power.

While the previous equations characterize the triple cross-correlation, the autocorrelation amplitude can be defined by[4]

$$G(0) = \frac{\sum_i \eta_i^2 N_i}{(\sum_i \eta_i N_i)^2} \quad (6)$$

## RESULTS

For these proof-of-principle 3C-FCCS experiments, quantum dot labels were chosen because of their photostability, narrow emission spectra, and large two-photon excitation cross section.[14] It is well-known that QDs can blink, which can alter the shape of correlation decays resulting in misrepresentation of their concentrations.[15,16] However, we have found that by using low TPE rates, this effect can be mitigated since the altered shape of the autocorrelation decay (ACD) is related to excitation saturation.[16] To verify that our experiments were performed in the appropriate TPE regime, the excitation power dependence was measured for all nanoparticles. The results are shown in Figure 3. For the nanobarcode particle, signal from the 605 nm emission channel was the first to demonstrate saturation, at around 60 mW (measured immediately before entering the microscope), as shown in Figure 3, panels a and b. For the free QDs, the 605 nm emission dots also saturated first at around 60 mW as shown in Figure 3, panels c and d. Therefore, the excitation power was kept at or below 50 mW for all experiments.

Sample correlation decays for powers above and below saturation are given in Figure 3. Similar to previous studies, the ACDs showed signs of blinking behavior, indicated by a lack of plateau (which represents the correlation amplitude) at short lag times, at excitation powers above 60 mW (Figure 3a). At excitation powers of 50 mW or below, the ACDs displayed the usual plateaus. The overall three-color cross-correlation decay shape had no dependence on excitation power (Figure 3b), other than the usual, decreasing amplitude resulting from saturation as excitation power increases, as indicated in Figure 3, panels c and d.[16] Of note is the small feature at around 0.08 s in the three-color cross-correlation decays. This is an artifact due to electrical flicker noise in the laser. It does not affect the data analyses as these data are not included in the fitting process. Additionally, the two-dimensional (2-D) full three-color cross-correlation decays maintained the same square


dx.doi.org/10.1021/ac302572k | Anal. Chem. 2012, 84, 9623−9631

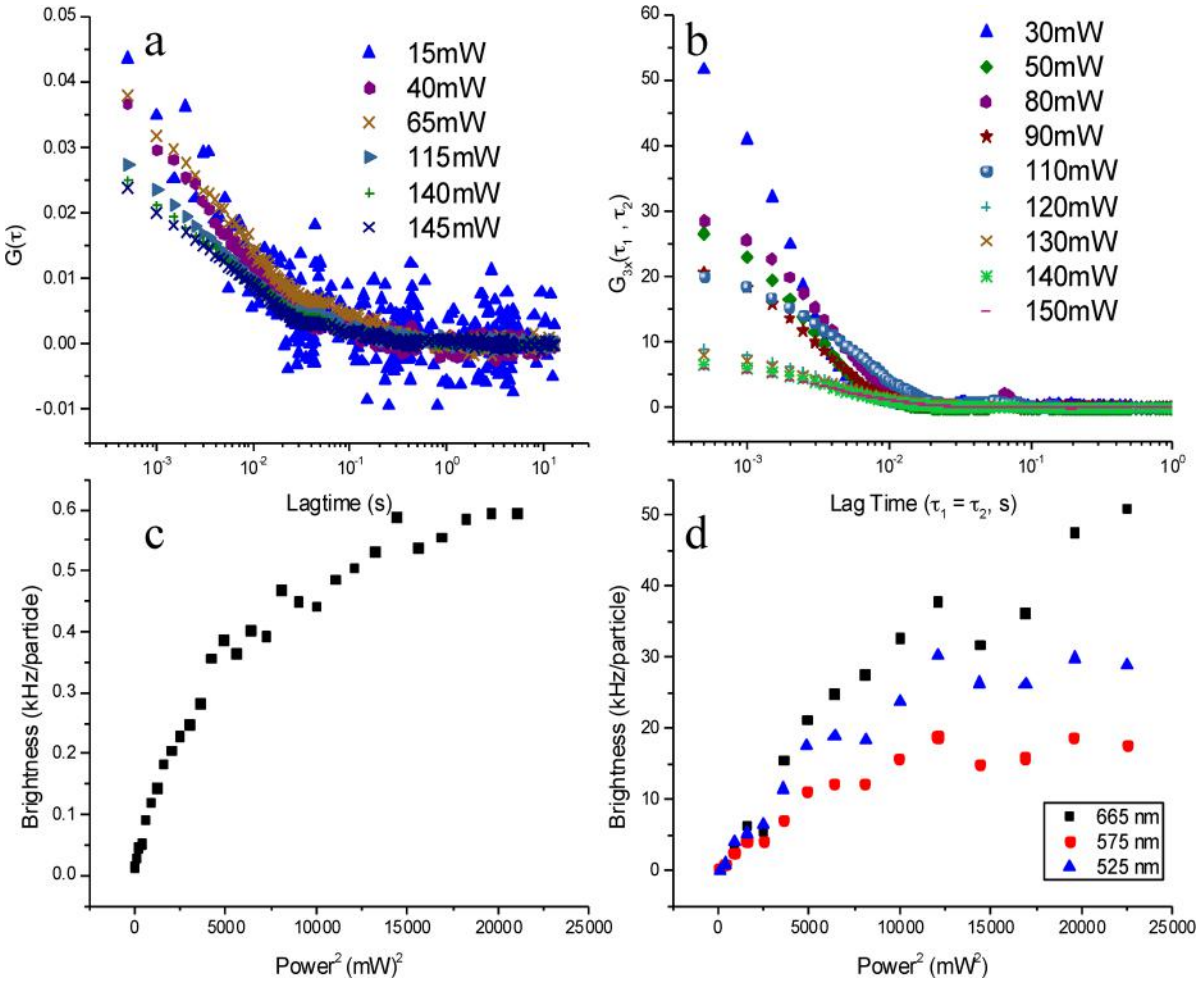


**Figure 3.** (a) Autocorrelation decays for the orange quantum dots (605 nm emission wavelength) at various laser excitation powers as noted in the legend. (b) Diagonal three-color cross-correlation decays for nanobarcode particles at various laser excitation powers as noted in the legend. (c) Plot of the brightness (counts/s/particle) of the 605 nm quantum dots as a function of laser power squared. (d) Plot of the brightness (counts/s/particle) of the nanobarcode particles as a function of laser power squared. Responses from the three detection wavelength channels are given independently.

shape at all powers (Supporting Information Figure S2). This indicates no interdependence of the order of multiplication ($\tau_1$ and $\tau_2$) in the three-color cross-correlation.[6] These data are consistent with previous studies where blinking does not affect the shape of the cross-correlation function because the blinking dynamics between different colored QDs is not correlated.[13]

In order to assess the sensitivity of 3C-FCCS to detect species with three labels in a background of single-color species, three-color nanobarcode particles were mixed in solutions with increasing concentrations of free QDs. Examples of the correlation decays are displayed in Figure 4. For example, Figure 4a shows a series of three-color cross-correlation decays of nanobarcode particles as a function of adding 2 $\mu$L aliquots of 100 nM freely diffusing 655 nm emitting QDs to the solution. The concentration range of the free QDs was chosen so that their signal starts near the fluorescence intensity of the nanobarcode particles and ends at a concentration ratio near 100:1 of free QDs to nanobarcodes. It is notable that the amplitude of the 3C-FCCS decay decreases with an increasing background of free QDs, as was expected from eq 3. Even with the largest background, the decay was still easily measured, meaning that a fit could be performed on the decay and that it was detectable using a 10 s data collection run (see Figure 5). Since the volumes being added (2−14 $\mu$L) were a small fraction of total volume of solution (200 $\mu$L), there was effectively no volume change.

Panels b−d of Figure 4 display the ACDs for the three color channels. The ACDs for the 655 nm channel are given in Figure 4b and show a similar downward trend in correlation amplitudes as in panel a, but instead follow eq 6. By contrast, panels c and d of Figure 4 should show no change in amplitude, as these represent the 525 and 605 nm channels, respectively. This was mainly the case compared with Figure 4b; however, there was a slight degree of scatter in the amplitudes, which may have resulted from small amounts of aggregation of the nanobarcode particles. Panels e−g of Figure 4 depict the averaged intensity scans for 0, 6, and 10 $\mu$L aliquots of 655 nm QDs added to the nanobarcode particle solution. Note the increase in the red trace, which represents the 655 nm channel, until it is more than a factor of 10 greater than the original solution. Similar data (not shown) were collected from experiments where backgrounds of 605 or 525 nm emitting QDs were added to a solution of nanobarcode particles with similar findings.

Figure 5 shows examples of 3C-FCCS triple cross-correlation decay data and a fit to the data using eq 2. Figure 5a displays a


dx.doi.org/10.1021/ac302572k | Anal. Chem. 2012, 84, 9623−9631

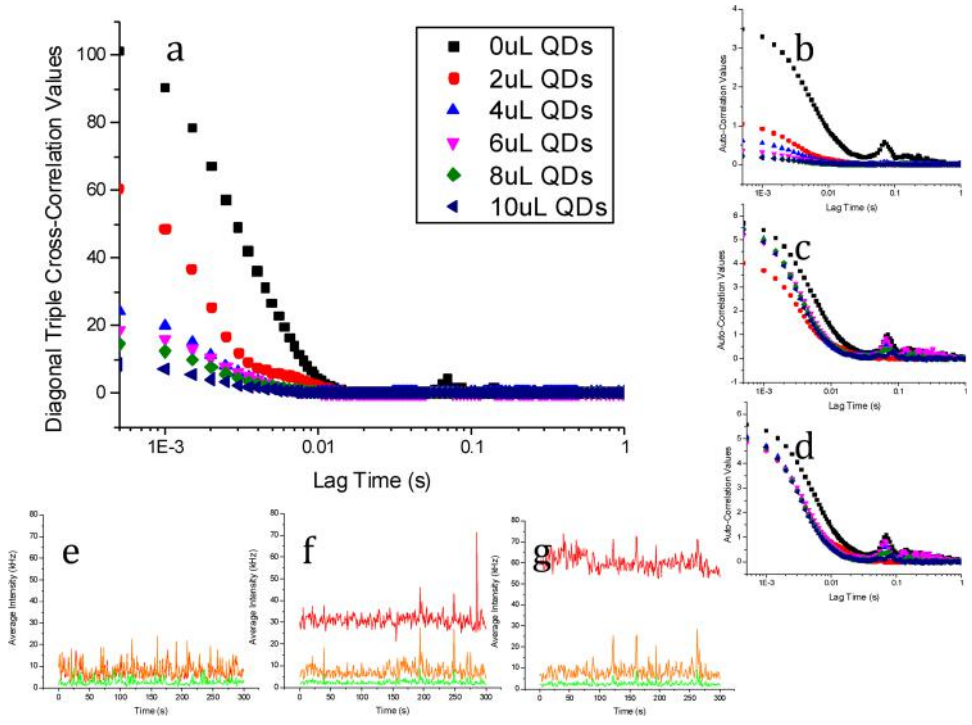


**Figure 4.** (a) Diagonal $G_{3x}(\tau_1, \tau_2)$ decays for various additions of free 655 nm emitting QDs. The volumes of the QDs added are given in the legend. Total solution volume is 200 $\mu$L. (b) Autocorrelation decays for signal from the 655 nm channel. (c) Autocorrelation decays for signal from the 605 nm channel. (d) Autocorrelation decays for signal from the 525 nm channel. (e–g) Count rate trajectories (655 nm, red; 605 nm, orange; 525, green) for the nanobarcode particle solutions with the addition of 0, 6, and 10 $\mu$L of 655 nm emitting QDs, respectively.

nanobarcode particle solution with 14 $\mu$L of (10 nM) 655 nm emitting QDs added. The fit using eq 2[7] is clearly more representative of the data than the standard cross-correlation decay model.[13] From the decay time, $\tau_D$, and a calibrated TPE volume, the diffusion coefficient, $D$, for the nanobarcode particles can be obtained. The diffusion coefficient can then be inputted into the Stokes–Einstein equation to estimate the hydrodynamic radius of the particles. This produces an $r_H$ of 80 ± 5 nm, which is in good agreement with the values of hydrodynamic radius from DLS and dehydrated radius SEM (83 ± 0.6 nm and 69 ± 3 nm, respectively).

Figure 5b contains two plots of 3C-FCCS decays for nanobarcode particles with 8 $\mu$L background of 655 nm emitting QDs. The black squares represent a typical data collection run of 300 s. By comparison, the red points result from a data collection run of 10 s.

To verify that eqs 3–5 could be applied to environments containing free QDs and three-color nanobarcode particles, several series of solutions were examined. They included nanobarcode solutions with backgrounds of all individual single-colored free QDs separately, as well as a background of three different colored individual QDs combined in one solution. The decays were plotted and fit as in Figure 5 for each series. The amplitudes of these decays were measured and then plotted against the volume of free QDs added to the original solution. The plots were then assessed using eq 5, where the brightness per particle, $\eta$, was calculated from the average fluorescence count rates and the $G(0)$'s of the isolated nanoparticles and QDs. The plots of these series are shown in Figures 6–9.

In Figure 6a, three data runs were collected for each addition of free red QDs to a nanobarcode particle solution. The data (represented by black squares) show a decreasing trend of $G_{3x}(0, 0)$ as more free red QDs were added to the solution. In general, this was expected because the denominator in eq 3 would increase. The precise shape of the trend was modeled using eq 5 (represented by magenta circles). The two plots compare very well, certainly within the measurement error. Panels b–d of Figure 8 are the autocorrelation amplitudes ($G(0)$'s) for the 655, 525, and 605 nm signals, respectively. One expects that only the 655 nm amplitudes would change, since adding 655 nm emitting QDs affects only this channel.

Figures 7 and 8 show the results of adding 525 and 605 nm QDs to solutions of three-color nanobarcode beads, respectively. The amplitudes of the 3C-FCCS decays follow the same trends as in the previous figure and are well-modeled using eq 5. The trends in the autocorrelation amplitudes for these data suggest both that there is good spectral separation of signal and that the volume of solution added is small enough such that the measured trends are unaffected, with one exception. Panels b–d of Figure 8 are the autocorrelation amplitudes ($G(0)$'s) for the 605, 525, and 655 nm signals, respectively. One expects that only the 605 nm amplitudes would change, since adding 605 nm emitting QDs affects only this channel. This is largely true, with the possible exception of a minor decrease in the 655 nm amplitude, possibly due to a small degree of cross talk of the 605 nm dots into the 655 nm channel.

As a final and more complex assay, we added all three colors of free QDs to the nanobarcode particle solution. A plot of the resulting amplitudes is shown in Figure 9. In panels b–d of Figure 9 we have displayed an example of a 3C-FCCS decay for the highest concentration of free QDs. Under these conditions (an 800:1 ratio of free dots/nanobarcode particles), the signal-to-noise ratio of the decay is excellent.

Since the applicability of eqs 3 and 6 has been demonstrated for these well-controlled solutions, the concentrations of all


dx.doi.org/10.1021/ac302572k | Anal. Chem. 2012, 84, 9623–9631

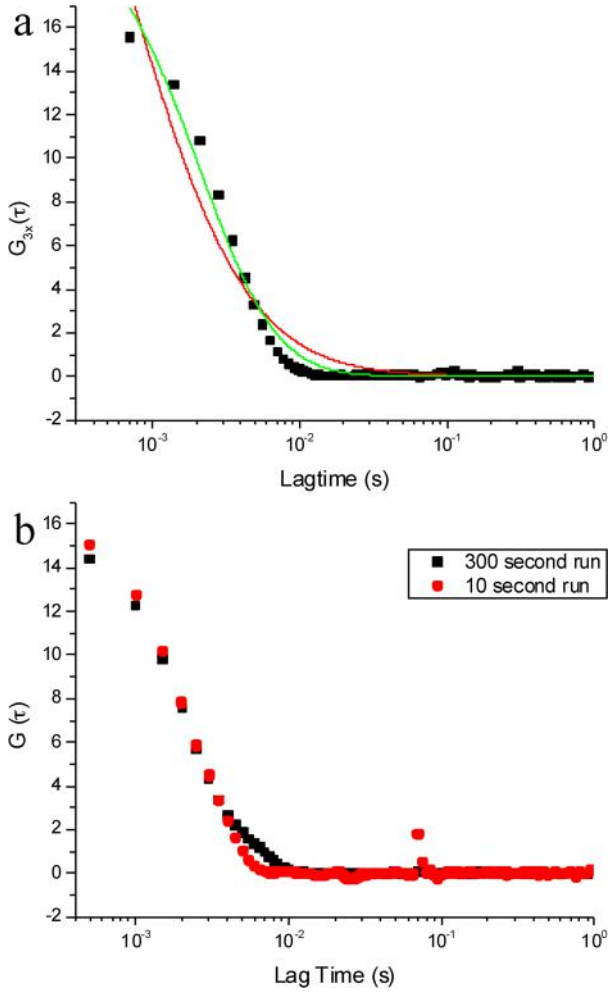


**Figure 5.** (a) Plot of diagonal $G_{3x}(\tau_1, \tau_2)$ decay (squares) and fit to the data using eq 5 (green line) for the aforementioned nanobarcode particle solution with 8 $\mu$L of 655 nm QDs added. The red line is the best fit using the standard FCCS decay term (ref 13). (b) Plot of diagonal $G_{3x}(\tau_1, \tau_2)$ decay for a solution of nanobarcode particles with 8 $\mu$L of 605 emitting QDs added. Data collection times were 300 s (black squares) and 10 s (red dots).

species in an unknown mixture can be determined. To do this, we can solve eqs 3 and 6 using Ridders' method[17] to return the numbers of particles in the TPE volume, $N_{abc}$, $N_a$, $N_b$, and $N_c$ if the brightnesses of all the particles are known and the amplitudes of the correlations have been measured. The results of this analysis (for the same controlled mixtures as above) are displayed in Table 1. The calculated values agree very well with those known from the serial additions noted.

## DISCUSSION

We examined the utility of 3C-FCCS to determine the concentrations of complex mixtures of nanoparticles, with emphasis on direct measurement of three-color nanobarcode particles in a background of single-color nanoparticles. Since one can accurately control the relative concentrations of these species, we can test the approaches and theories developed for 3C-FCCS with high confidence. Clearly, the data can be collected over a short time period, which suggests that 3C-FCCS will be applicable to measuring kinetics of association or dissociation in a large background of free particles.

The approach here relies on our ability to measure and model three-color cross-correlation decays rapidly. In Figure 5b it is noteworthy that the model and data do not overlap perfectly. This is most likely owing to some degree of polydispersity in the size and brightness of nanobarcode particles, which could arise naturally and from a small degree of permanent aggregation. Nevertheless, the amplitudes reproduce appropriate trends in concentrations as we will see later in this section. And also the decay times produce reasonable size information about the particles. The polydispersity would affect any size measurement and therefore does not limit this approach. In the future, a model which sums over the polydispersity could be applied, but such models are challenging to use, as one must have a priori knowledge of system. Therefore, the model is appropriate for the purposes of this study.

It is possible to detect three-color nanobarcode particles at concentrations of 10 pM with a greater than 800:1 background of single-color particles (Figure 9) in less than 10 s (Figure 5b). The QDs used in this assay are bright; however, if we were to use organic fluorophores, the sensitivity would likely decrease by no more than an order of magnitude. We can compare our results with those of Heinze et al.,[4] who analyzed triple coincidence of three fluorescently tagged oligonucleotides binding to a common complementary single strand of DNA, and Hwang et al., who studied ternary streptavidin–biotin interactions by pairwise FCCS.[5] The Heinze et al. study indicated that 0.5 nM ternary DNA complexes were detectable in a background of approximately 70 nM three-color oligonucleotides in 6 s. Since our experimental setup is very similar to that of Heinze et al., the higher sensitivity in our experiments is most likely due to the larger brightness of the QDs.[4] A main advantage of the current approach is that 3C-FCCS provides direct and immediate confirmation of bound three-color species, without the need of data analysis and deconvolution. Since we calculate the complete triple cross-correlation decay, our approach provides size information on the three-color species, which the aforementioned coincidence analysis cannot. The pairwise FCCS approach of Hwang et al. does provide size information, since the full two-color FCCS decay is used, but their approach only infers the existence of three-color bound species through elegant mathematical fitting of the data.[5] It will always remain possible, using pairwise FCCS, to mistakenly identify three-color species.

Our 3C-FCCS approach can also be compared with MC-FRET. In recent years, there have been several sophisticated studies of complex molecular associations using FRET. Kim et al. examined agonist and antagonist binding to the estrogen receptor using one-donor, three-acceptor FRET.[9] Their results are compelling, and the mathematical deconvolution of the direct excitation was facilitated by taking ratios of acceptor emission in a pairwise fashion. All FRET studies have the potential to be hampered by changes in donor–acceptor orientation that mimics changes in distance. 3C-FCCS is much less sensitive to such phenomena. A significant advantage of FRET is the donor–acceptor distance information it provides. Although 3C-FCCS does not provide this, it does report on the overall hydrodynamic size of the triply labeled species. The appropriateness of one technique versus the other should be based on the application.

Lastly, we must comment on the method for extraction of parameters from the equations modeling the data. The Ridders' method,[17] used for determining the amounts of singly and


dx.doi.org/10.1021/ac302572k | Anal. Chem. 2012, 84, 9623–9631

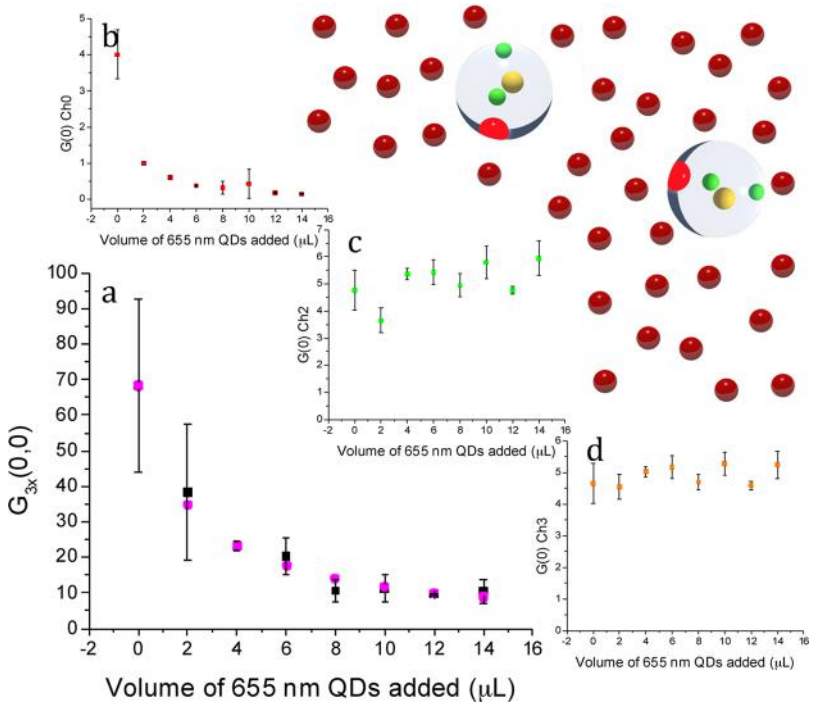


**Figure 6.** (a) $G_{3x}(0, 0)$ values as a function of volume of 655 nm QDs added to the nanobarcode particle solution. The measured values are given by the black squares. The magenta circles represent the values predicted using eq 5 as described in the text. (b) $G(0)$ values for the data gathered in the 655 nm detection channel. (c) $G(0)$ values for the data gathered in the 525 nm detection channel. (d) $G(0)$ values for the data gathered in the 605 nm detection channel. Error bars represent the standard deviations derived from three different experiments. The cartoon is a schematic depiction of the solution contents.

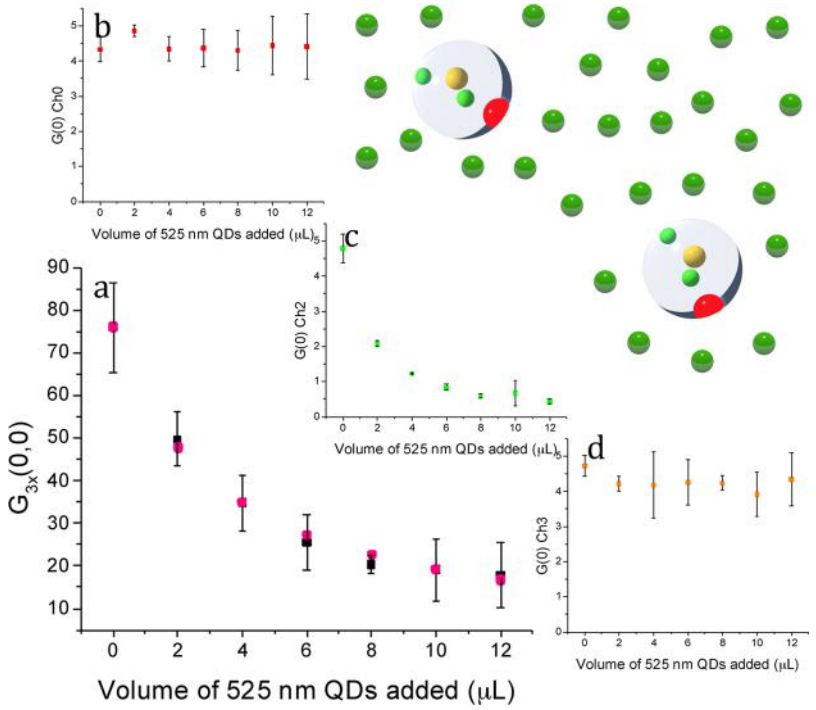


**Figure 7.** (a) $G_{3x}(0, 0)$ values as a function of volume of 525 nm QDs added to the nanobarcode particle solution. The measured values are given by the black squares. The magenta circles represent the values predicted using eq 5 as described in the text. (b) $G(0)$ values for the data gathered in the 655 nm detection channel. (c) $G(0)$ values for the data gathered in the 525 nm detection channel. (d) $G(0)$ values for the data gathered in the 605 nm detection channel. Error bars represent the standard deviations derived from three different experiments. The cartoon is a schematic depiction of the solution contents.

triply labeled species ($N_a$, $N_b$, $N_c$, and $N_{abc}$), is a numerical solution for simultaneous equations (6−9). For a typical kinetics experiment (as we will explore in a subsequent study), single time points would be measured, and therefore, the


dx.doi.org/10.1021/ac302572k | *Anal. Chem.* 2012, 84, 9623−9631

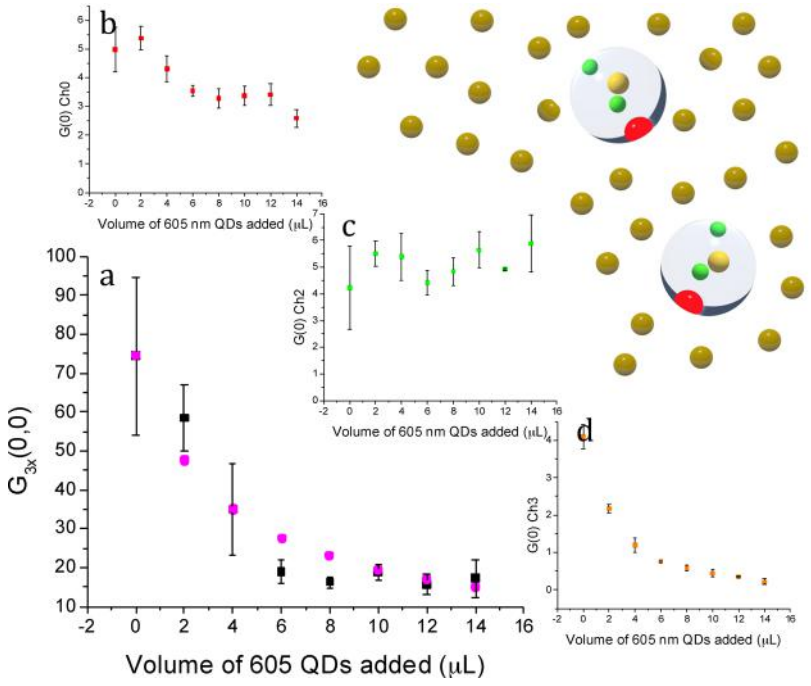


**Figure 8.** (a) $G_{3x}(0, 0)$ values as a function of volume of 605 nm QDs added to the nanobarcode particle solution. The measured values are given by the black squares. The magenta circles represent the values predicted using eq 5 as described in the text. (b) $G(0)$ values for the data gathered in the 655 nm detection channel. (c) $G(0)$ values for the data gathered in the 525 nm detection channel. (d) $G(0)$ values for the data gathered in the 605 nm detection channel. Error bars represent the standard deviations derived from three different experiments. The cartoon is a schematic depiction of the solution contents.

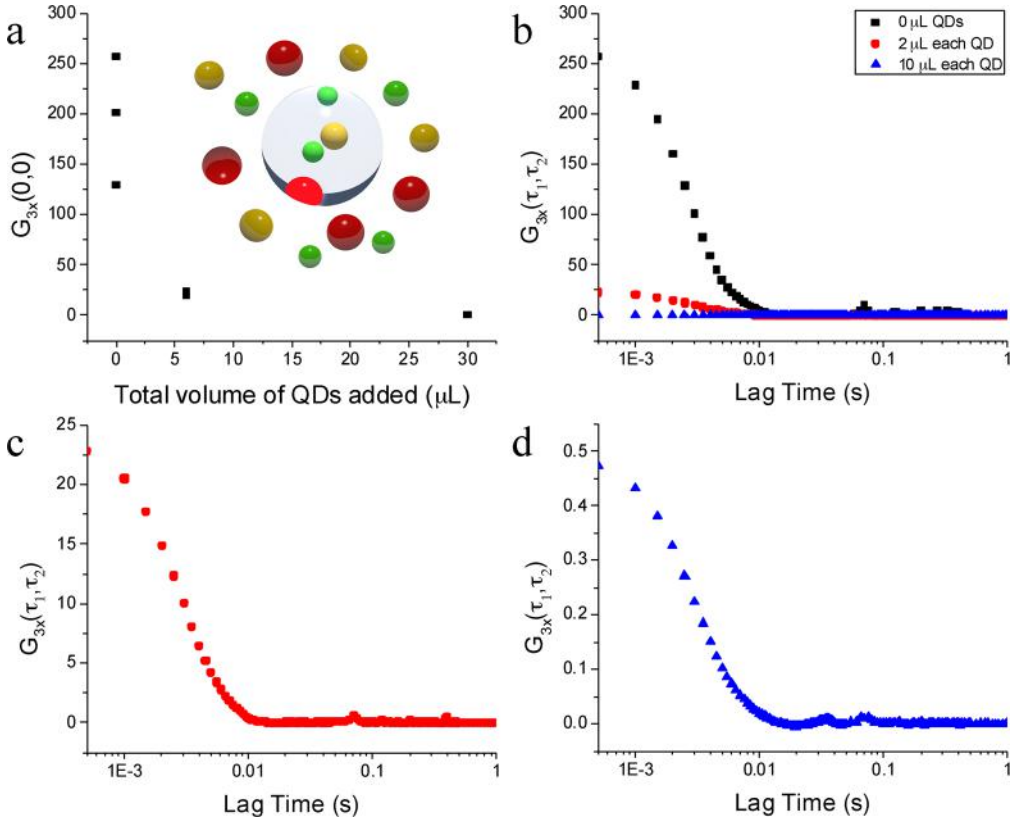


**Figure 9.** (a) $G_{3x}(0, 0)$ values as a function of volume of total QDs (525, 605, and 655 nm in equal volumes) added to the solution of nanobarcode particles. The cartoon is a schematic depiction of the solution contents. (b) Plots of diagonal $G_{3x}(\tau_1, \tau_2)$ decays for the addition of all three individual, single-colored QDs. (c) Expanded plot of the diagonal $G_{3x}(\tau_1, \tau_2)$ decay for a 2 $\mu$L addition. (d) Expanded plot of the diagonal $G_{3x}(\tau_1, \tau_2)$ decay for a 10 $\mu$L addition. See text for details.


dx.doi.org/10.1021/ac302572k | *Anal. Chem.* 2012, 84, 9623−9631

Table 1. Values Determined from Simultaneous Solution of Eqs 3 and 6

| | I | | II | | III | | IV | |
|---|---|---|---|---|---|---|---|---|
| | measured | predicted | measured | predicted | measured | predicted | measured | predicted |
| $N_{rog}$ | 0.11 | 0.10 | 0.10 | 0.10 | 0.11 | 0.10 | 0.06 | 0.07 |
| $N_r$ | 10 | 10 | | | | | 16 | 15 |
| $N_o$ | | | 2.1 | 2.0 | | | 21 | 20 |
| $N_g$ | | | | | 1.1 | 1.0 | 21 | 20 |

accuracy of the $N$ values will depend on the accuracy of the $G(0)$'s. The accuracy of the latter is determined by the signal-to-noise ratio of the correlation decays, which is typically greater than 10:1. Other studies have used a global fitting approach to fluorescence correlation spectroscopy (FCS) analysis of complex mixtures.[18,19] In these other approaches the entire correlation decays were fit using the appropriate equations and the Levenberg–Marquardt method. A Levenberg–Marquardt method is best when the parameters are, in principle, overdetermined due to the large number of data points in the decays. In our current study, we were more concerned with the amplitudes of the decays being measured simultaneously, which justifies the use of Ridders' method since fewer data points per parameter were available.

## CONCLUSIONS

We have demonstrated that 3C-FCCS can be used to simultaneously determine the concentrations of all species in complex nanoparticle solutions including singly and triply labeled species. The 3C-FCCS method has not been previously validated in this way, where the concentrations of all species are known a priori. Moreover, since we calculate the full triple cross-correlation decay, our method can be used to determine the size of the triply labeled species. This approach can now be used to investigate complex assembly and disassembly kinetics for a wide variety of applications. These include the self-assembly of higher-order nanoparticles, as well as innumerable biological applications such as the DNA repair mechanism previously mentioned. Since 3C-FCCS permits sensitive, real-time tracking of association kinetics, we anticipate that this will permit a predictive understanding of these important processes with detail previously unavailable.

## ASSOCIATED CONTENT

### Supporting Information

Additional information as noted in text. This material is available free of charge via the Internet at http://pubs.acs.org.

## AUTHOR INFORMATION


### Corresponding Author

*Phone: 403-220-3226. E-mail: dcramb@ucalgaryu.ca.

### Present Address

[§]Laboratory for Stem Cells and Tissue Engineering, Department of Biomedical Engineering, Columbia University, 622 West 168th Street, Vanderbilt Clinic 12-234, New York, NY 10032.


### Notes

The authors declare no competing financial interest.

## ACKNOWLEDGMENTS

We are grateful to NSERC and CIHR for funding this research through the AGENO and CHRP programs. M.L.B. and H.M.W. thank NSERC and the University of Calgary, respectively, for scholarship support. The authors are indebted to Professor Simon Trudel (Calgary) for generating the nanoparticle graphics. We are indebted to Andy Read, Joel Schrieber, and Todd Willis for design and fabrication of the detection filter cube.

## REFERENCES


(1) Mann, S. *Nat. Mater.* **2009**, *8* (10), 781–792.
(2) Wang, L.; Tan, W. H. *Nano Lett.* **2006**, *6* (1), 84–88.
(3) Clamme, J. P.; Deniz, A. A. *Chem. Phys. Chem.* **2005**, *6*, 74.
(4) Heinze, K. G.; Jahnz, M.; Schwille, P. *Biophys. J.* **2004**, *86* (1), 506–516.
(5) Hwang, L. C.; Gosch, M.; Lasser, T.; Wohland, T. *Biophys. J.* **2006**, *91* (2), 715–727.
(6) Wobma, H. M.; Blades, M. L.; Grekova, E.; McGuire, D. L.; Chen, K.; Chan, W. C. W.; Cramb, D. T. *Phys. Chem. Chem. Phys.* **2012**, *14* (10), 3290–3294.
(7) Ridgeway, W. K.; Millar, D. P.; Williamson, J. R. *J. Phys. Chem. B* **2012**, *116* (6), 1908–1919.
(8) Shcherbakova, D. M.; Hink, M. A.; Joosen, L.; Gadella, T. W. J.; Verkhusha, V. V. *J. Am. Chem. Soc.* **2012**, *134* (18), 7913–7923.
(9) Kim, S. H.; Gunther, J. R.; Katzenellenbogen, J. A. *J. Am. Chem. Soc.* **2010**, *132* (13), 4685–4692.
(10) Galperin, E.; Verkhusha, V.; Sorkin, A. *Nat. Methods* **2004**, *1* (3), 209–217.
(11) Giri, S.; Sykes, E. A.; Jennings, T. L.; Chan, W. C. W. *ACS Nano* **2011**, *5* (3), 1580–1587.
(12) Giri, S.; Li, D. W.; Chan, W. C. W. *Chem. Commun. (Cambridge, U. K.)* **2011**, *47* (14), 4195–4197.
(13) Swift, J. L.; Heuff, R.; Cramb, D. T. *Biophys. J.* **2006**, *90* (4), 1396–1410.
(14) Larson, D. R.; Zipfel, W. R.; Williams, R. M.; Clark, S. W.; Bruchez, M. P.; Wise, F. W.; Webb, W. W. *Science* **2003**, *300* (5624), 1434–1436.
(15) Doose, S.; Tsay, J. M.; Pinaud, F.; Weiss, S. *Anal. Chem.* **2005**, *77* (7), 2235–2242.
(16) Heuff, R. F.; Marrocco, M.; Cramb, D. T. *J. Phys. Chem. C* **2007**, *111* (51), 18942–18949.
(17) Ridders, C. J. F. *IEEE Trans. Circuits Syst.* **1979**, *26* (11), 979–980.
(18) Previte, M. J. R.; Pelet, S.; Kim, K. H.; Buehler, C.; So, P. T. C. *Anal. Chem.* **2008**, *80* (9), 3277–3284.
(19) Eggeling, C.; Kask, P.; Winkler, D.; Jager, S. *Biophys. J.* **2005**, *89* (1), 605–618.